

New Radiometers: SMOS

A Dual Pol L-band 2D Aperture Synthesis Radiometer¹

Y. Kerr¹, J. Font², P. Waldteufel³, A. Camps⁴, J.Bará⁴, I.Corbella⁴, F. Torres⁴, N. Duffo⁴, M. Vall.Ilossera⁴, G. Caudal³

¹ CESBIO(CNES, CNRS, UPS), 18 Av. Édouard Belin, 31401 Toulouse Cedex 4, France, tel. (33) 561558522,

Yann.Kerr@cesbio.cnes.fr

²Institut de Ciències del Mar/CSIC, P. Joan de Borbó s/n, 08039 Barcelona, Spain, tel. (34) 932216416,

jfont@icm.csic.es

³IPSL, 10-12 Av. de l'Europe, 78140 Vélizy, France, tel. (33) 0139254818,

Philippe.Waldteufel@cetp.ipsl.fr, Gerard.Caudal@cetp.ipsl.fr

⁴Universitat Politècnica de Catalunya, Campus Nord, D3, tel (34) 934016849,

camps@tsc.upc.es, bara@tsc.upc.es, corbella@tsc.upc.es, xtorres@tsc.upc.es, duffo@tsc.upc.es, merce@tsc.upc.es

Abstract—Since the mid '80s, aperture synthesis interferometric radiometers have received increased attention to monitor the Earth at low microwave frequencies (L-band), where there is a maximum sensitivity to soil moisture and ocean salinity.

At L-band, classic radiometers require large steerable antennas to meet the spatial resolution requirements (30-50 km at most, 10-20 km wished for), from a low polar orbit platform.

During the '90s, technological studies were conducted by the European Space Agency (ESA) with an eye to design a 2-D synthetic aperture L-Band radiometer (the Microwave Imaging Radiometer by Aperture Synthesis project: MIRAS). In the fall of 1998, in answer to a call for Earth Explorer Opportunity Missions issued by ESA, the Soil Moisture and Ocean Salinity Mission proposal (SMOS), based upon a radiometer concept derived from the MIRAS studies, was submitted. In May 1999, following a selection procedure, ESA approved the SMOS mission for an extended phase A.

This paper is organized as follows:

TABLE OF CONTENTS

1. INTRODUCTION
2. THE SMOS BASIC CONCEPT
3. INSTRUMENT PERFORMANCE
4. MODELING INSTRUMENT IMPERFECTIONS
5. ERROR CORRECTION AND IMAGE RECONSTRUCTION
6. SMOS FIELD OF VIEW AT SURFACE LEVEL; MULTIANGULAR PARAMETER RETRIEVAL
7. PERFORMANCE CRITERIA AND OPTIMIZATION
8. CONCLUSIONS

1. INTRODUCTION

Significant progress in terms of weather forecasting, climate monitoring and extreme events forecasting rely on a better quantification of both Soil Moisture (SM) and Sea Surface Salinity (SSS). Several recent group and workshop reports conclude that further improvements now depend upon the availability of global observational information on SM and SSS.

It is now well recognized that on land, water and energy fluxes at the surface/atmosphere interface are strongly dependent upon Soil Moisture (SM). Evaporation, infiltration and runoff are driven by SM while soil moisture in the root zone governs the rate of water uptake by vegetation. SM is thus a key variable in the hydrologic cycle. SM and its spatio-temporal evolution as such is an important variable for numerical weather and climate models, and should be accounted for in hydrology and vegetation monitoring.

For oceans, SSS plays an important role, for example, in the Northern Atlantic sub polar area, where intrusions with a low salinity influence the deep thermohaline circulation and the meridional heat transport. Variations in salinity also influence the near-surface dynamics of tropical oceans, where rainfall modifies the buoyancy of the surface layer and the tropical ocean-atmosphere heat fluxes. SSS fields and their seasonal and inter-annual variabilities are thus tracers and constraints on the water cycle and on the coupled ocean-atmosphere models.

Even though both SM and SSS are used in predictive atmospheric, oceanographic, and hydrologic models, no capability exists to date to measure directly and globally these key variables. Since in situ measurements are very far from global, the only hope of achieving this relies in a dedicated space mission.

Passive microwaves are established as the most efficient mean to monitor SM and SSS. The protected region of the electromagnetic spectrum within the L-band (1.4 -1.427 GHz) offers unique opportunities for measuring these two important Earth science variables (i.e., SM and SSS) that cannot be achieved in other regions of the spectrum.

¹ 0-7803-5846-5/00/\$10.00 © 2000 IEEE

One of the most significant drawbacks of L-Band radiometry, however, is that it implies the use of very large antennas and a spaceborne L-band instrument thus creates a significant technological challenge. Even though the concept was proved by early L band space experiments, such as the one on SKYLAB back in the 70s, no dedicated space mission followed, because achieving a suitable ground resolution ($\leq 50\text{-}60$ km) required a prohibitive antenna size (≥ 4 m). All the research work was consequently performed using either ground or airborne radiometers.

Recent development of the so-called interferometry design, inspired from the very large baseline antenna concept (radio astronomy), makes such a venture possible. The idea consists of deploying small receivers in space (located on a deployable structure), then reconstructing a brightness temperature (T_B) field with a resolution corresponding to the spacing between the outmost receivers. The idea was put forward by D. LeVine et al., in the '80's (the Electrically Steered Thinned Array Radiometer project: ESTAR) and validated with an airborne system. In Europe, an improved concept was next proposed to ESA. While MIRAS capitalizes on the ESTAR design, it embodies major improvements. The two-dimensional MIRAS interferometer allows measuring T_B at large incidences, for two polarizations. Moreover, the instrument images a whole scene in just 0.3 s, which corresponds to an image blur of 2.2 km, less than 10% the smallest pixel size. As the satellite moves, a given point within the 2D field of view is observed from different view angles. A series of independent measurements is then obtained, which allows to retrieve surface parameters with much improved accuracy [1].

It is in this perspective that the SMOS mission was proposed [2], [3]. It is a mission with broad and ambitious scientific objectives. In addition, it can also be considered as a demonstrator, which should allow both to assess the potential of L-Band 2D interferometric radiometry for possible operational uses, and to pave the way for future, upgraded technical implementations.

It is also expected that the SMOS mission will provide significant information on vegetation water content, which will be very useful for regional estimates of crop production. Finally, significant research progress is expected over the cryosphere, through improving the assessment of the snow mantle, and of the multi-layered ice structure. These quantities are of significant importance to the global change issue. Research on sea ice will also be carried out.

SMOS aims at providing, over the open ocean, global salinity maps with an accuracy better than 0.1 PSU every few days, with a 200 km spatial resolution; over the land surfaces, global maps of soil moisture, with an accuracy better than $0.035 \text{ m}^3/\text{m}^3$ every 3 days, with a space resolution better than 60 km, as well as vegetation water content with an accuracy of 0.2 kgm^{-2} . The platform would be on a sun synchronous orbit (6 a.m.) at 757 km height. Table 1 summarizes its main parameters.

Such an ambitious and innovative concept implies significant work on the instrumental concept and mission design. This paper aims at depicting the current state of the art and showing methods developed to optimize the use of

the 2-D radiometer with respect to the scientific objectives, and to suggest ways to optimize the instrument characteristics and mission elements.

Table 1 Main parameters of the SMOS mission

Parameter	Value
Size	~ 4.5 m each arm
Weight	175 kgr
Power consumption	220 W
Swath	620 km
Spatial resolution	30 – 90 km
Radiometric sensitivity	0.8 – 2.2 K
Absolute radiometric accuracy	< 3 K
Foreseen launch date	2005

2. THE SMOS BASIC CONCEPT

Interferometric radiometers measure the complex cross-correlation between the signals $b_1(t)$ and $b_2(t)$ collected by the pairs of antennas than can be formed in a sparse array (Figure 1).

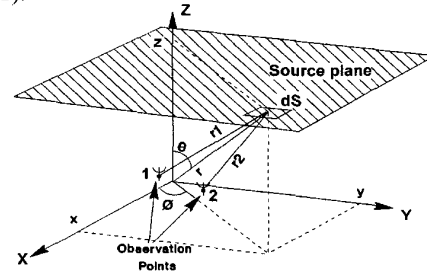


Figure 1 Two antennas of an interferometric radiometer forming a baseline

The antennas are assumed to be placed over the XY plane at $(x_{1,2}, y_{1,2})$, and each correlation is a sample of the so called visibility function $V(u, v)$ (Kelvin) [4,5]:

$$\begin{aligned}
 V_{1,2}(u_{1,2}, v_{1,2}) &= \frac{1}{k_B \sqrt{B_1 B_2} \sqrt{G_1 G_2}} \frac{1}{2} \langle b_1(t) b_2^*(t) \rangle = \\
 &= \frac{1}{\sqrt{\Omega_1 \Omega_2}} \iint_{\xi^2 + \eta^2 \leq 1} \frac{T_B(\xi, \eta)}{\sqrt{1 - \xi^2 - \eta^2}} F_{n1}(\xi, \eta) F_{n2}^*(\xi, \eta) \\
 &\quad \tilde{\gamma}_{1,2} \left(-\frac{u_{1,2}\xi + v_{1,2}\eta}{f_0} \right) \exp(-j 2\pi (u_{1,2}\xi + v_{1,2}\eta)) d\xi d\eta, \quad (1)
 \end{aligned}$$

where $(u_{1,2}, v_{1,2}) = (x_2 - x_1, y_2 - y_1) / \lambda$ is the normalized spacing between the antennas, $(\xi, \eta) = (\sin \theta \cos \phi, \sin \theta \sin \phi)$ are the directional cosines with respect X and Y, $T_B(\xi, \eta)$ is the brightness temperature (Kelvin), $F_{n1,2}(\xi, \eta)$ is the normalized antenna voltage pattern (without units), k_B is the Boltzman's constant, $\Omega_{1,2}$ is the solid angle of the antenna radiation pattern, $G_{1,2}$ is the gain of the receiving channel, and the fringe-wash function, that accounts for spatial decorrelation effects, is given by

$$\begin{aligned}
 \tilde{\gamma}_{1,2}(t) &= \frac{e^{-j2\pi f t}}{\sqrt{B_1 B_2}} \int_0^{f_m} H_{n1}(f) H_{n2}^*(f) \exp(j 2\pi f t) df, \quad (2) \\
 B_{1,2} &= \int_0^{f_m} |H_{n1,2}(f)|^2 df.
 \end{aligned}$$

where $H_{n1,2}(f)$ is the normalized frequency response of receivers 1 and 2, f_0 is their center frequency, and $B_{1,2}$ is the noise bandwidth.

For an ideal interferometer (identical receivers and antennas), and negligible decorrelation effects ($\tilde{r}_{12}(r) \approx 1$), Equation (1) reduces to a Fourier transform between the visibility function and the brightness temperature weighted by the antenna radiation pattern. The brightness temperature is a two-dimensional function restricted to the unit circle $\xi^2 + \eta^2 \leq 1$. Consequently, its Fourier transform (visibility function) can be sampled in an optimal way over a hexagonal grid, leading to the largest alias free Field Of View (FOV), for a determined spacing between the antennas. The rectangular sampling provided by T-, U-, or L- shaped arrays requires an antenna spacing of $d=1/2$ wavelengths for alias-free operation, while the hexagonal sampling provided by a Y-, or triangular shaped arrays, requires only $d=1/\sqrt{3}$ wavelengths. It allows a reduction of 13.4 % of the required visibility samples and the associated hardware [6,7]. If due to technological limitations (antenna size and antenna mutual coupling) the minimum baseline cannot be equal to $1/\sqrt{3}$ wavelengths, the alias free field of view (FOV) is then limited by the periodic repetition of the unit circle centered at $(1/\sqrt{3}d, 1/d)$, $(1/\sqrt{3}d, -1/d)$, $(-1/\sqrt{3}d, 1/d)$, $(-1/\sqrt{3}d, -1/d)$, $(2/\sqrt{3}d, 0)$, and $(-2/\sqrt{3}d, 0)$ [7]. However, a large part of the unit radius circle is occupied by the sky, and some pre-processing techniques can then be applied [8] to enlarge the alias-free FOV up to the Earth-sky border (Figure 2).

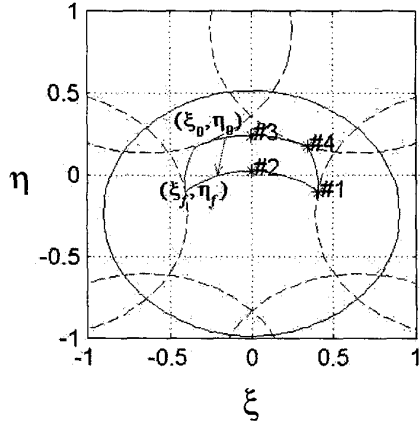


Figure 2. Earth contour (continuous line) and Earth aliases (dashed lines) limiting the alias free field of view for an SMOS-type instrument at a height=639Km, tilted at an angle $\beta=34^\circ$, and $d=0.89$ wavelengths. The indicated FOV of interest has a swath width of 725 Km and ranges from ground incidence angles from 40° to 55° . (ξ_0, η_0) and (ξ_f, η_f) indicate the initial and final positions of a pixel as it travels through the FOV of interest.

Among them, the optimum angular resolution is achieved by the Y-array, which is the configuration selected for SMOS (Figure 3) [9].

3. INSTRUMENT PERFORMANCE

Angular resolution

The angular resolution is determined by the (u, v) spatial frequency coverage, which is shown in Figure 4. For this star-shaped (u, v) coverage, the half-power width of the synthesized beam in the directional cosines domain is approximately given by [10]

$$\Delta \xi_{\rightarrow \delta \theta}^{\text{rect}} \approx \frac{\pi/2}{\Delta u_{\text{max}}}, \quad (3)$$

where $\Delta u_{\text{max}} = 2\sqrt{3}N_{EL} d$ is the maximum distance in wavelengths between (u, v) points (Figure 4). When the visibility samples are tapered (apodization), the synthetic beamwidth is enlarged, the side lobes are reduced, and the main beam efficiency is improved. For $N_{EL} = 23$ antennas per arm, spaced $d=0.89$ wavelengths, the computed half-power beam widths are 1.43° , 1.80° and 2.11° , for the rectangular (no window), Hamming, and Blackmann windows (with rotational symmetry). At the points marked as 1, 2, 3 and 4 (Figure 2) these values lead to on-ground cross-track spatial resolutions ranging from ~ 30 km to ~ 37 km, and radial spatial resolutions from ~ 39 km to ~ 66 km.

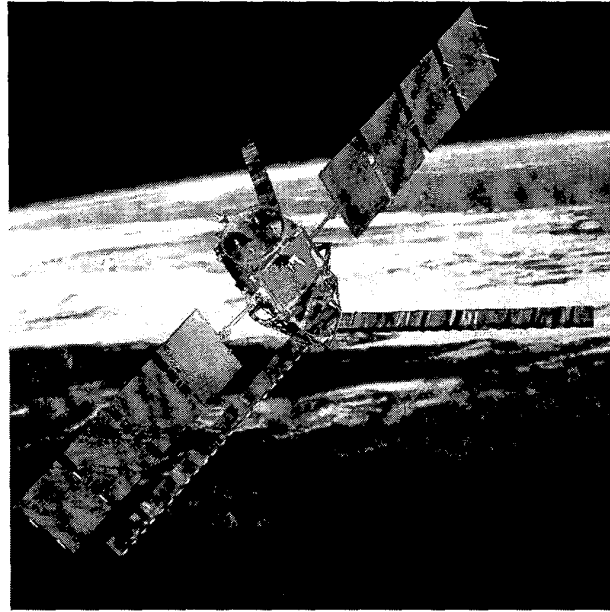


Figure 3. Artist's view of SMOS.

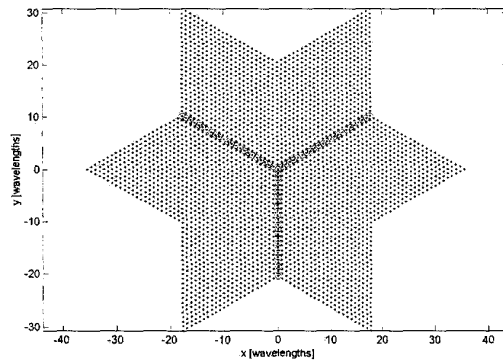


Figure 4 (u, v) spatial frequency coverage associated with a 23 antennas per arm Y-array spaced $d=0.89$ wavelengths.

Radiometric sensitivity

Assuming identical receivers with a Gaussian frequency response, the radiometric sensitivity close to the antenna boresight is [5, 11]

$$\Delta T = \Omega \frac{\sqrt{3} d^2}{2} \frac{T_{sys}}{\sqrt{B\tau_{eff}}} \sqrt{N_r} \frac{\alpha_w \alpha_{LO}}{\alpha_f} \quad (4)$$

where $T_{sys} = T_A + T_R$ is the system's temperature, T_A is the antenna temperature, T_R is the receivers' noise temperature, $\tau_{eff} = \tau/Q$ is the effective integration time, $Q=2.46$ for 1 bit/2 level digital correlators and samples taken at Nyquist rate [12], $N_r = 6N_{EL}^2 + 6N_{EL} + 1$ is the number of different (u,v) points, $0.45 \leq \alpha_w \leq 1$ is a parameter that depends on the window or apodization function used to taper the visibility samples, $1 \leq \alpha_{LO} \leq 1.41$ is a parameter that depends on the type of demodulation used, and $1 \leq \alpha_f \leq 1.19$ is a parameter that depends on filters' shape.

For the parameters of the proposed SMOS instrument [9], and a brightness temperature of 200K, the predicted radiometric sensitivity for each snapshot is 9.4 K, 5.3 K and 4.2 K, for the rectangular, Hamming and Blackmann windows. Except for the rectangular window, which exhibits very high side lobe levels, the product of the angular resolution times the radiometric sensitivity is approximately constant, which is known as the synthetic aperture interferometric radiometer uncertainty principle [11].

4. MODELING INSTRUMENT IMPERFECTIONS

The block diagram of an interferometric radiometer is shown in Figure 5.

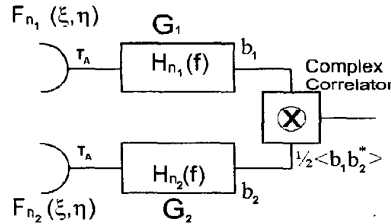


Figure 5 Baseline diagram: two receivers and correlator

Note that the filters $H_{1,2}(f)$ (not normalized) may include several amplifiers, filters and frequency conversions. The cross-correlation between the signals $b_1(t) = i_1(t) + j q_1(t)$ and $b_2(t) = i_2(t) + j q_2(t)$ is performed at base-band after coherent in-phase/quadrature (I/Q) demodulation, or numerically after sampling the signals centered at a small intermediate frequency. In SMOS, 1 bit / 2 level (1B/2L) digital correlators are foreseen because of their low power consumption, high speed, and high degree of integration, at the expense of a reduction of the effective integration time.

The output of 1B/2L correlators is not directly the complex visibility, but an intermediate magnitude $Z_{r,i}$ related to the normalized visibility by [12]

$$Z_r = \langle \text{sign}[i_i(t)] \text{sign}[i_i(t)] \rangle = \frac{2}{\pi} \arcsin(\mu_r) \quad (5a)$$

$$Z_j = \langle \text{sign}[q_i(t)] \text{sign}[i_i(t)] \rangle = \frac{2}{\pi} \arcsin(\mu_j) \quad (5b)$$

$$\mu_{ij} = \mu_r + j \mu_j = \frac{V_{ij}(u,v)}{\sqrt{T_{sysik} T_{sysj}}} \quad (6)$$

where $\text{sign}[x]$ is the sign function. A total-power radiometer is required to measure the sample $V(0,0) = T_A$, assumed to be the same for all the antennas, to be included in T_{sys} (Equation (6)). Errors can be classified according to their impact on the measured visibility samples and their correction/calibration procedure, independently of the subsystem that generates them.

Antenna errors

Antenna errors affect the exploration of the scene (Equation 1) [13-15], and can only be accounted for by measuring them on the ground and including them in the inversion algorithm. Antenna imperfections are antenna pattern phase and amplitude mismatches (usually in form of ripples), antenna coupling, antenna pattern pointing errors, position errors and the cross-polarization ratio. Most of these errors can be kept under control provided mechanical tolerances are small, as compared to the wavelength (not specially critical at L-band). However, the errors induced by antenna coupling errors are unavoidable. To first order, coupling effects produce a mixing (linear combination) of the visibility samples that will be measured in coupling-free conditions. Higher order effects account for multiple reflections in the array structure and produce a non-linear combination of the visibility samples [14], which complicates the image reconstruction process [8].

Channel errors

Channel errors (or separable errors) appear as separate gain factors or phase addends at the visibility samples and require antenna-based calibration procedures. These errors are due to in-phase channel errors (filters' phase, time delays, etc.), I/Q demodulators quadrature errors, and channel gain errors [16]. Channel errors can be calibrated by most methods: distributed noise injection, redundant space calibration, etc., provided baseline errors are small. Long intercalibration periods require thermal control of the electronics to minimize drifts.

Baseline errors

Baseline errors (or non-separable errors) cannot be separated into gain factors or phase addends related to antenna channel parameters and require baseline-based calibration procedures requiring the injection of correlated noise simultaneously to all the antennas. These kind of errors are phase/amplitude errors due to frequency response mismatches, offsets generated by the correlation of common LO leakage, comparators threshold mismatches and jitter in the 1B/2L digital correlators [17] etc. Frequency response mismatches can be controlled by specifying an attenuation mask to be satisfied by all receivers (to be computed numerically for each particular type of filter). In addition techniques have been devised to dynamically measure the shape of the fringe-washing function within the accuracy required to achieved the final radiometric accuracy [18].

Once corrected, the measured radiation voltage patterns of the antennas assembled in the array, and the measured fringe-washing functions are used in Equation 1 to find out the brightness temperature distribution.

5. ERROR CORRECTION AND IMAGE RECONSTRUCTION

Offset baseline errors are calibrated by switching the receivers' input from the antennas to a matched load (uncorrelated noise injection). Then, channel or separable errors are calibrated by a hardware scheme based on a distributed noise-injection network [19-21], which is schematically sketched in Figure 6.

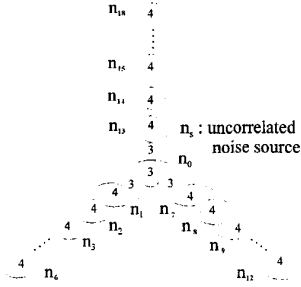


Figure 6 Distributed noise injection network. The central noise source drives the 12 central antennas. Each source drives correlated noise to a set of 8 adjacent antennas

By switching the antennas to a central noise source, correlated thermal noise is injected to the twelve central antennas (the first three of each arm plus the three additional ones in the center of the array), allowing the track of phase/amplitude among the arms. Then, by sequentially turning on and off the odd and the even noise sources (Figure 7), phase and amplitude relationships can be established between sets of non-overlapping groups of eight adjacent receivers.

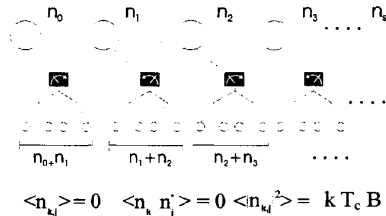


Figure 7 Noise distribution scheme. Even and odd noise sources drive sequentially correlated noise to a set of eight adjacent antennas

Once offset baseline errors and channel phase/amplitude error terms have been corrected, the image reconstruction algorithm decomposes the visibility samples in three terms. The first one comes from the sky, the second one from a fictitious constant brightness temperature body at temperature T_{earth} inside the Earth field of view, and the third one, $\Delta V(u, v)$, contains the variations of the brightness temperature over this constant background [8], which are the ones to be found out by the iterative algorithm. Note that the image reconstruction is only possible in the alias-free central region, a kind of hexagon with curved sides (Figure 2).

Table 2 summarizes the different error sources and their contribution to the snap-shot radiometric accuracy and sensitivity (0.3 s integration time). Since each pixel appears N_{look} times in the FOV, simulation results have shown an improvement by a factor $\sqrt{N_{look}}$ in the thermal noise and errors induced by oscillations of the arms of the Y-array. A much smaller improvement, in the range 1.16 to 1.32, depending on the windowing and the spatial frequency

content of the scene being imaged scene, is expected for the rest.

Table 2 Instrument residual errors after calibration, instrument's radiometric accuracy (systematic errors, mean value for pixels in the FOV) and radiometric sensitivity (random errors, mean value for pixels in theFOV) ($T_{AH}=300K$, $T_{AV}=200K$).

ERROR SOURCE	RADIOMETRIC ACCURACY	RADIOMETRIC SENSITIVITY
PHYSICAL LIMITATIONS		
- discretization and windowing	0.02 K	
- thermal noise ($\tau=0.3$ s)		4.18 K (snap-shot)
SYSTEM IMPERFECTIONS		
ANTENNA ERRORS		
• Phase ripple ($\sigma_\phi=0.34^\circ$)	0.50 K	
• Amplitude ripple ($\sigma_A=0.5\%$)	0.53 K	
• Pointing ($\sigma_\theta=0.15^\circ$)	0.20 K	
• In-plane oscillations (5 mm)		0.10 K
• Off-plane oscillations (5 mm)		0.06 K
• V/H cross-talk (X-Pol 25 dB)	0.16 K (H)	0.63 K (V)
CHANNEL ERRORS		
• In-phase & I/Q ($\sigma_\phi=0.1^\circ$)	0.04 K	
• Amplitude errors (Dicke radiometer)	0.02 K	
• Amplitude errors ($\Delta\mu_{ij}$) ($\sigma_{\Delta TR}=1.25$ K)	0.25 K	
BASELINE ERRORS		
• Residual Offset (LO) ($\sigma_{offset}=1.5 \cdot 10^{-6}$)	0.07 K	
• Filter's phase errors ($\phi_{12}=0.43^\circ$)	0.18 K	
• Filter's amplitude errors ($\Delta\mu_{ij}=0.002$)	0.20 K	
• Digital Correlators Threshold errors	-	
• Delay errors ¹⁰ : $\Delta f=15\text{MHz}\pm 0.2\text{MHz}$ $B=30\text{MHz}$, $t_d=2\text{ns}$ Phase error: 5.4° pre-cal, 0.1° cal	0.03 K	
• Quadrature error: 0.7° pre-cal	0.18 K	
TOTAL (quadratic summation)	0.88 K (H-POL) 1.07K (V-POL) (SNAP-SHOT)	4.18 K (SNAP-SHOT)

6. SMOS FIELD OF VIEW AT SURFACE LEVEL; MULTIANGULAR PARAMETER RETRIEVAL

Figure 2 presented the field of view defined by directional cosines. As indicated in Section 2, the limits of the (extended) alias free zone are due to replicas of the Earth visibility zone. Figure 8 illustrates how the instantaneous FOV appears at Earth's surface [22].

The general topography is similar, although the aliasing boundaries, previously ellipses, have become more complicated curves. Since the antenna plane is tilted, the FOV is elongated ahead of the antenna, and conversely reduced beyond it.

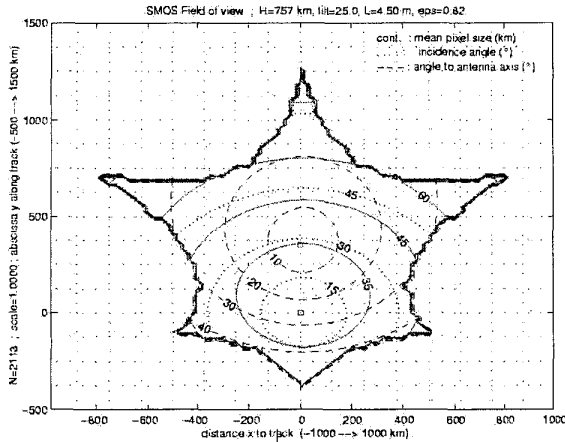


Figure 8 Instantaneous field of view for a representative SMOS configuration. A spherical Earth is assumed. Main parameters (flight altitude, arm length, tilting angle of the antenna plane, element spacing ratio) are indicated at the top of diagram. The vertical (y) axis is parallel to satellite motion; the subsatellite point as well as intersection of the antenna axis with Earth's surface are shown. Space resolution contours correspond to the average between radial and transverse angular 3dB widths, assuming a Gaussian spread point function; the smearing effect due to the satellite motion is neglected.

Three families of contouring curves are shown, respectively for incidence angle i , look angle with respect to the antenna axis θ_a , and space resolution Δs . These families are distinct, due to the antenna tilt.

Multangular Parameter Retrieval.

When considering the performances of the SMOS mission, the relevance of space resolution is obvious. The θ_a angle plays a part in determining space resolution; furthermore, the elementary antenna radiation pattern has to be accounted for when computing the radiometric sensitivity. Finally, the power radiated by Earth target areas depends on the incidence angle for each polarization.

The instantaneous FOV is two-dimensional: over every elementary observation period, SMOS provides a set of visibility functions that ultimately allow obtaining a 2D map for brightness temperatures T_B . As the satellites moves ahead, this means that each Earth area within the FOV will be seen several times, for varying incidence angles. This can be understood by drawing lines parallel to the vertical (y) axis on Figure 8 for various abscissas x away from the subsatellite track: such lines cross the incidence angle i contours.

In terms of soil moisture retrieval, this feature may be of considerable interest [1]. First, it supplies an increased number of independent samples; second, it allows improved discrimination between unknown surface parameters, inasmuch as they induce specific, distinct T_B variations as i varies.

The theory for the dependence of radiated power on surface soil moisture is well established for smooth cultivated areas or grass lands [23]. Based on this, retrieval algorithms

making use of T_B data for both polarizations and a range of incidence angles can be built. Three physical parameters are of main importance: soil moisture w_s , optical thickness of vegetation cover τ_v and surface temperature T_s .

While the main objective of SMOS on a land surface is to monitor soil moisture, w_s [3], the vegetation optical thickness is also of interest; besides, ancillary information for τ_v is inaccurate and difficult to obtain. On the other hand, a wealth of surface temperature data is available. Therefore it seems appropriate to retrieve both w_s and τ_v from SMOS data, assuming T_s is known from external sources with a specific uncertainty.

Figure 9 illustrates major features of the performances of such a retrieving method. Actually, the adjustment to simulated data is carried out assuming all three parameters are unknown, but taking into account the value supplied for T_s as well as the corresponding measurement error.

The uncertainty $\sigma(w_s)$ is seen to depend on three characteristics of the incidence angle sampling: it decreases with increasing number, mean angle and range. As all three quantities vary across the FOV, this has to be taken into account when estimating SMOS performances. In the following section, the dependence of $\sigma(w_s)$ upon incidence mean angle and range will be accounted for using an empirically adjusted function.

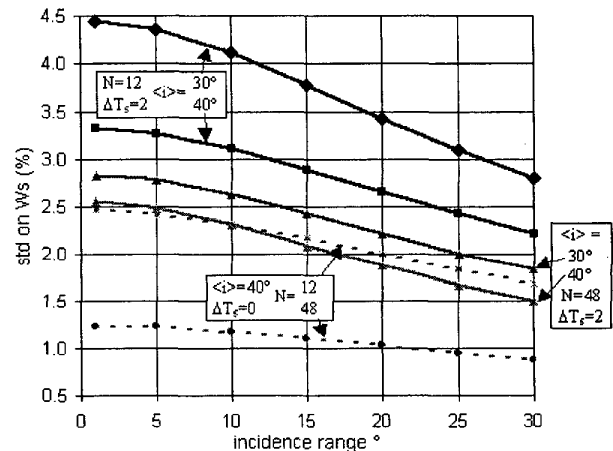


Figure 9 Random uncertainties over soil moisture retrieved from SMOS simulated data. For each curve are indicated the number N of available T_b data for each polarization, the mean incidence angle $\langle i \rangle$, and the uncertainty ΔT_s over T_s . The available i values are assumed to be spread regularly over a varying range (along the abscissa). Note the effect of the T_s estimated uncertainty: if T_s were perfectly known (dotted curves), $\sigma(w_s)$ would vary exactly as the inverse square root of the number of samples. Target characteristics are $w_s=0.2$, $\tau_v=2.6$, $T_s=280$ K.

7. PERFORMANCE CRITERIA AND OPTIMIZATION

Three main criteria are needed to summarize the performance of SMOS over land surfaces: space resolution, accuracy, time sampling interval.

Space Resolution

There is no unique way to define the space resolution. Furthermore, no detailed analysis has been carried out up to

now on the way to deal with space resolution(s) varying inside the set of T_B measurements used for w_s retrieval at a given distance x across the FOV. Such effects will have to be investigated considering the space structure of the moisture field, and looking at the best way to take advantage of oversampling. In any case, it is clear that any representative space resolution worsens as x increases.

This will eventually bound the SMOS swath, because scientific reasons set a limit Δs_m to the acceptable space resolution over land surfaces. Specifically, the useful FOV region will be bounded by either the aliasing limits or a contour for space resolution Δs_m , whichever comes first. Figure 8 (see e.g. the 60 km contour) illustrates the impact of a Δs_m threshold.

Accuracy

The accuracy over w_s measurements is a major scientific requirement of the SMOS mission; the simplest way to state it is to say that the error should not exceed a maximum value w_{sm} . This first translates into accuracy requirements for the measured T_B . Absolute accuracy depends on both errors due to imperfect instrument stability and calibration, and random measurement errors. We do not consider in this section the former (although of course this is a major issue); then the basic source of uncertainty is the radiometric sensitivity ΔT . In addition, effects related to the multiangular retrieval process have to be considered.

From the previous sections, it is clear that the overall performance, in terms of retrieved w_s estimates, is best close to the sub-satellite track, and worsens as the distance x to this track across the FOV increases. Indeed three phenomena contribute to this variation: the number of available independent samples decreases; the average elementary antenna gain decreases; the range of available incidence angles is reduced. The only positive effect (due an increase of the mean incidence angle) is not likely to reverse this trend.

Time Sampling Interval

Then, assuming the space resolution requirement is met by restricting the FOV as indicated above, the useful half swath X_m is the maximum x value for which $\sigma(w_s)$ stays below w_{sm} .

In this way, requirements on space resolution and accuracy are combined so as to yield a maximum value of the actual swath. This is convenient, because the swath is closely linked to the mean revisit time, and therefore to the mean time sampling interval $\langle \Delta t \rangle$.

The time sampling requirement that matters most concerns the maximum time interval Δt_m rather than its mean value. Obtaining Δt_m from $\langle \Delta t \rangle$ will require a detailed analysis of the satellite orbit. Still, since the average relationship between both quantities is obviously monotonous, looking for average values is a sensible way of optimizing the revisit time performance. It may certainly happen that the optimum obtained in this manner occurs for a flight altitude which does not provide the optimal revisit time; this would call for a further iteration phase.

There are other ways to characterize the overall performance of SMOS than setting threshold requirements; for example, it will certainly be worth looking at mean

values, for space resolutions and measurement accuracy, across the useful swath.

Figure 10 illustrates qualitatively, in the case of the satellite flight altitude, how this approach can be used for optimizing the SMOS configuration. For this particular parameter at least, the interesting feature is the existence of an optimal range of values.

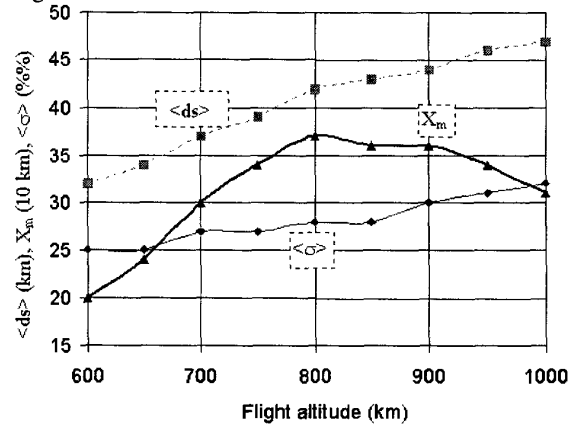


Figure 10 An example of variation of the maximum SMOS half swath X_m with flight altitude, showing an optimal range around 800-900 km. Selected space resolution threshold and w_s uncertainty requirements are 60 km and $0.04 \text{ m}^3/\text{m}^3$, respectively. Also shown are the space resolution $\langle ds \rangle$ and standard deviation $\langle \sigma \rangle$ of measured w_s , averaged across the whole selected swath. Other specified parameters are : tilt angle = 20° , arm length = 4.5 m, element spacing ratio = 0.80. The numerical results should be considered as indicative.

8. CONCLUSIONS

The 2-D, dual-polarized, aperture synthesis radiometer offers a unique opportunity to fill two glaring gaps in surface variable fields. The instrument concept is innovative and ambitious. Between the early 90's, when the concept was first formulated, and now considerable progress has been made on various aspects, including signal processing and algorithms, science, and technical development. These enabled the proposal of a mature and feasible SMOS concept to ESA. This paper has summarized part of the work carried out both on the interferometric radiometry concept and with respect to the optimization of the instrument configuration. Moreover, several studies are under way on the physics of measurements (inversion algorithms, SSS retrievals) and data assimilation to retrieve root zone soil moisture. Several field experiments are being planned or are under way.

In other words, as almost no satellite data is available at L band, the existing algorithms have been developed from ground based or airborne measurements. Most of the theoretical aspects are now covered and well established for many types of targets. The probability of having a space system will obviously foster research to unprecedented levels. Full use of instrument demonstrators will enable the fine-tuning of retrieval algorithms. Major issues which remain to be solved during the period before launch will be to address the scaling issues (this being currently done on a theoretical basis only) and the influence of wind speed on SSS retrieval. The mission being very innovating, current

knowledge does not allow us to always have clear-cut answers. The known issues have been investigated and solutions proposed. The next step will consist in carrying out suitable field experiments to validate the solutions and check whether all has been accounted for. Also, a SMOS simulator has been developed at Polytechnic University of Catalonia (UPC) in Spain. This tool should enable to build scenes from input data and could be used to check the error propagation when part of the system is deficient, and/or to deliver scenes for algorithm development and tests. The SMOS concept will be a demonstrator of L band measurements over the globe, paving the way to more ambitious concepts in terms of spatial resolution or frequency range. SMOS will undoubtedly make available long needed measurements of surface soil moisture, vegetation biomass and sea surface salinity and foster new research in these fields as well as in cryospheric studies. SMOS should be launched as a second Earth Explorer Opportunity Mission, tentatively in 2005.

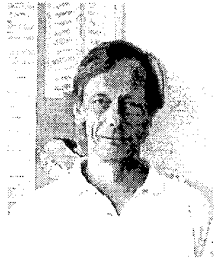
ACKNOWLEDGEMENTS

Much of this paper summarizes work carried out in the frame of the MIRAS project of the ESTEC technology program. This research has been also supported by the Spanish Research Program CICYT, and the French CNRS and CNES.

REFERENCES

- [1] Wigneron, J.P., P. Waldteufel, A. Chanzy, J. C. Calvet, O. Marloie, Hanocq, and Y. Kerr, "Retrieval capabilities of L-Band 2-D interferometric radiometry over land surfaces (SMOS Mission)", *6th Specialist Meeting on Microwaves Radiometry*, VSP, Zeist, The Netherlands, in press, 1999.
- [2] Beljaars, A. C., M. Viterbo, M. J. Miller, and A. K. Betts, The anomalous rainfall over the USA during 1993: sensitivity to land surface parameterization, *Mon. Wea.Rev.*, 124 : 362-383, 1996.
- [3] Kerr, Y., P. Waldteufel, J. P. Wigneron, J. M. Martinuzzi, B. Lazard, J. M. Goutoule, C. Tabard, A. Lannes, "The Soil Moisture and Ocean Salinity Mission: an overview", *6th Specialist Meeting on Microwaves Radiometry*, VSP, Zeist, The Netherlands, in press, 1999.
- [4] Thompson, A. R., J. M. Moran, and G. W. Swenson, *Interferometry and Synthesis in Radio Astronomy*, John Wiley and Sons, 1986.
- [5] Ruf, C. S., C. T. Swift, A. B. Tanner, D. M. LeVine, "Interferometric Synthetic Aperture Radiometry for the Remote Sensing of the Earth", *IEEE Trans. on Geoscience and Remote Sensing*, Vol. 26, N° 5, pp 597-611, September 1988.
- [6] Mersereau, R. M., "The Processing of Hexagonally Sampled Signals", *Proceedings of the IEEE*, Vol 67, N° 6, pp 930-949, June 1979.
- [7] Camps, A., J. Bará, I. Corbella, F. Torres, "The Processing of Hexagonally Sampled Signals with Standard Rectangular Techniques: Application to 2D Large Aperture Synthesis Interferometric Radiometers", *IEEE Transactions on Geoscience and Remote Sensing*, GRS-35, No 1, pp 183-190, January 1997.
- [8] Camps, A., J. Bará, F. Torres, I. Corbella, "Extension of the CLEAN Technique to the Microwave Imaging of Continuous Thermal Sources by Means of Aperture Synthesis Radiometers", *Progress In Electromagnetics Research*, PIER 18, pp 67-83, January 1998.
- [9] Kerr et al., 1998, MIRAS on RAMSES: radiometry applied to soil moisture and salinity measurements, Full proposal, A.O. Earth Explorer Opportunity Missions, ESA, 1998. SMOS web site: <http://www-sv.cict.fr/cesbio/smos>
- [10] Bará, J., A. Camps, F. Torres, I. Corbella, "Angular Resolution of two-dimensional hexagonally sampled interferometric radiometers", *Radio Science*, Vol 33, No 5, pp 1459-1473, September-October 1998.
- [11] Camps, A., I. Corbella, J. Bará, F. Torres, "Radiometric Sensitivity Computation in Aperture Synthesis Interferometric Radiometry", *IEEE Transactions on Geoscience and Remote Sensing*, GRS-35, No 2, pp 680-685, March 1998. (errata corrected in GRS-35, No 5, September 1998).
- [12] Hagen, J., and D. Farley, Digital correlation techniques in radio science, *Radio Science*, Vol. 8, No 8-9, 775-784, August-September 1973.
- [13] LeVine, D.M. and D.E. Weissman, Calibration of synthetic aperture radiometers in space: Antenna effects, in *Proceedings of the International Geoscience and Remote Sensing Symposium, IGARSS '96*, pp. 878-880, IEEE Press, Piscataway, N.J., 1996.
- [14] Camps, A., J. Bará, F. Torres, I. Corbella, J. Romeu, "Impact of Antenna Errors on the Radiometric Accuracy of Large Aperture Synthesis radiometers. Study Applied to MIRAS", *Radio Science*, Vol. 32, No 2, pp 657-668, March-April 1997.
- [15] Camps, A., F. Torres, I. Corbella, J. Bará, P. de Paco, "Mutual Coupling Effects on Antenna Radiation Pattern : An Experimental Study Applied to Interferometric Radiometers", *Radio Science*, Vol 33, No 6, pp 1543-1552, November-December 1998.
- [16] Torres, F., A. Camps, J. Bará, I. Corbella, "Impact of Receiver Errors on the Radiometric Resolution of Large 2D Aperture Synthesis Radiometers. Study Applied to MIRAS", *Radio Science*, Vol 32, No1-2., pp 629-642, March-April 1997.
- [17] Camps, A., F. Torres, I. Corbella, J. Bará, J. A. Lluch, "Threshold and Timing Errors of 1 bit/2 level Digital Correlators in Earth Observation Synthetic Aperture Radiometry", *Electronics Letters*, Vol 33, No 9, pp 821-813, April 1997.
- [18] Camps, A., F. Torres, J. Bará, I. Corbella, F. Monzón, "Automatic calibration of channels frequency response in interferometric radiometers", *Electronics Letters*, Vol 35, No 2, pp 115-116, January 1999.
- [19] Torres, F., A. Camps, J. Bará, I. Corbella, R. Ferrero, "On-Board Phase and Modulus Calibration of Large Aperture Synthesis Radiometers: Study Applied to MIRAS", *IEEE Transactions on Geoscience and Remote Sensing*, GRS-34, No 4, pp 1000-1009, July 1996.
- [20] Corbella, I., A. Camps, F. Torres, J. Bará, "Analysis of noise injection networks for interferometric radiometer calibration", *IEEE Trans on Microwave Theory and Techniques*, in press.
- [21] Torres, F., A. Camps, I. Corbella, J. Bará, N. Duffo, M. Vall-llossera, "Calibration trade-off in large interferometric radiometers devoted to earth observation", *6th Specialist Meeting on Microwave Radiometry and Remote Sensing of the Environment*, March 1999, Florence, Italy, VSP, Zeist, The Netherlands, in press, 1999.
- [22] Waldteufel P., Anterrieu E., Goutoule J.M., Kerr Y., "Field of view characteristics of a 2-D interferometric antenna, as illustrated by the MIRAS/SMOS L-band concept", *6th Specialist Meeting on Microwaves Radiometry*, VSP, Zeist, The Netherlands, in press, 1999.
- [23] Wigneron J.P., Chanzy A., Calvet J.C. and N. Bruguier, "A simple algorithm to retrieve soil moisture and vegetation biomass using passive microwave measurements over crop fields", *Rem. Sens. Environ.*, 51, pp 331-341 (1995)

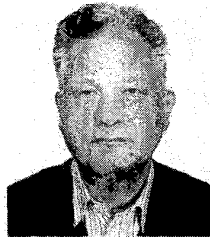
Yann H. Kerr (M'88) received the engineering degree from ENSAE, the M.Sc. from Glasgow University in E&EE, and Ph.D from Université Paul Sabatier. From 1980 to 1985 he was employed by CNES. In 1985 he joined LERTS. He spent 19 months at JPL, Pasadena in 1987-88. He has been working at CESBIO since 1995. His fields of interest are in the theory and techniques for microwave and thermal infrared remote sensing of the Earth, with emphasis on hydrology and vegetation monitoring. He was the science lead on the MIRAS project for ESA, and is the Lead-Investigator of the SMOS mission.



Jordi Font received the Licenciado (1973) and Doctor (1986) degrees in Physics from the University of Barcelona, Spain. Since 1987 he has been the responsible for the Physical Oceanography Group at the Institut de Ciències del Mar (CSIC, Spanish Council for Scientific Research), Barcelona, where he is Research Scientist and since 1996 serves as Assistant Director. His research interests are focused on marine circulation, upper ocean dynamics, and remote sensing of the ocean. Participant in 40 oceanographic campaigns. 100 communications to scientific symposia. 60 published papers. Co-Lead Investigator and responsible for the ocean salinity measurement within the SMOS Science Team.



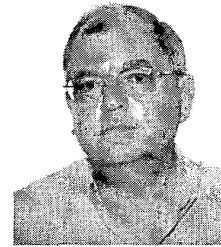
Philippe Waldteufel received a degree (1962) from École Polytechnique and a Doctorat d'État (1970) from the Université de Paris. He is a senior scientist at Centre National de la Recherche Scientifique. His main scientific interests have been ionospheric and thermospheric physics, radar meteorology, radiowave propagation, macroeconomics, and finally microwave radiometry. He has also served as Director of the Institut de Physique du Globe de Clermont-Ferrand, Deputy Director in the French Weather Service Research Department, and Director for Science in the French Research Ministry.



Adriano J. Camps received the degree of Ingeniero (1992) and Dr. Ingeniero in Telecommunications (1996), from the Polytechnic University of Catalonia, Barcelona, Spain. In 1991-1992, was at the ENS des Télécommunications de Bretagne, France. In 1993, Dr. Camps joined the Dept. of Signal Theory and Communications of the Polytechnic University of Catalonia (UPC), as an Assistant Professor, and as an Associate Professor since 1997. During 1999 he is on sabbatical at the Microwave Remote Sensing Laboratory, at the University of Massachusetts. His research interests are focused on interferometric and polarimetric microwave radiometry, mainly focused in the SMOS/MIRAS instrument.



Javier Bará received the Sc.M. E.E. degree (1968) and the Ph.D. E.E. degree (1972), from Brown University, Providence, R.I. Since 1972, he has been a Professor at the Polytechnic University of Catalonia (UPC), Barcelona, Spain, where he held several posts of academic responsibility as associate School Dean, Dean and Department Director. His research interests have been in the field of microwaves (ferrites, integrated circuits, satellite communications, industrial heating and drying processes) and is at present involved in projects in non-guided optical communications in the near infrared and interferometric radiometry for remote sensing of the Earth.



Ignasi Corbella received the Ingeniero (1977) and Doctor Ingeniero (1983) degrees in Telecommunication Engineering, both from the Polytechnic University of Catalonia (UPC), Barcelona, Spain. In 1976 he joined the School of Telecommunication Engineering in Barcelona as a Research Assistant in the Microwave Laboratory. He became assistant professor in 1982, Associate Professor in 1986 and Professor in 1993. During the school year 1998/99 he worked at NOAA/Environmental Technology Laboratory in Boulder (Colorado-USA) as a guest researcher, developing methods for radiometer calibration and data analysis. His research work include microwave airborne and satellite radiometry and microwave system design.



Francesc Torres received his Ingeniero (1988) and Doctor Ingeniero degree (1992) in Telecommunication Engineering, both from the Polytechnic University of Catalonia (UPC), Barcelona, Spain. In 1988-89 he was Research Assistant in the RF System Division at the European Space Agency, Holland, devoted to microwave device testing and characterization. In 1989 he joined the Antenna-Microwave-Radar group of the UPC, where he currently holds a post as Associate Professor. His main research interests are focused to the design and test of microwave systems and subsystems. He is currently engaged in research on interferometric radiometers devoted to Earth observation.



Núria Duffo. Telecommunication Engineer from the School of Telecommunications Engineering, Polytechnic University of Catalonia (UPC), Spain, in 1990. Doctor in Telecommunication Engineering from UPC, 1996. Since 1997, Associate Professor at UPC. Current research activities: numerical methods in electromagnetics, microwave radiometry, antenna analysis and design.



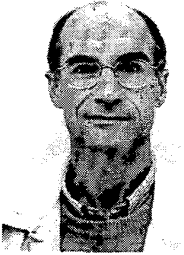
Mercè Vall.Ilossera,

Telecommunication Engineer from the School of Telecommunication Engineering, Polytechnic University of Catalonia (UPC, Barcelona, Spain), 1990. Doctor in Telecommunication Engineering from UPC, 1994. Since 1997, Associate Professor at UPC. Current research activities: numerical methods in



electromagnetics, microwave radiometry, antenna analysis and design. Spent a sabbatical year in Montreal with the scholarship of the "Programme Québécois de Bourses d'excellence" (1996-97): "Stages de Formation postdoctorale au Québec pour jeunes diplômés étrangers."

Gerard Caudal was born in 1953 in Lyon (France). He graduated from École Polytechnique in 1974, and from École Nationale Supérieure des Télécommunications in 1976. He served during 4 years as engineer in Telecommunications. He then became involved in research activities devoted principally to the observation of the terrestrial ionosphere by ground-based radar, and modeling studies



of the planetary ionosphere and magnetospheres. After passing a Ph D thesis in 1987, he joined a group of remote sensing, being mainly involved in the study of the ocean surface by radar remote sensing. He became Professor at the University of Versailles in 1993.